Laser surface alloying of a novel $Nb_{11.2}Cr_{22.2}Co_{22.2}Ni_{22.2}Cu_{22.2}$/TiN/VC composite coating: a preliminary parametric study

Ayo Alabi[1*], *Abimbola* Popoola[1], *Olawale* Popoola[2], and *Ntombi* Mathe[3]

[1]Chemical, Metallurgical and Materials Engineering, Faculty of Engineering and Built Environment, Tshwane University of Technology, P.M.B. X680, Pretoria, South Africa
[2]Center for Energy and Electric Power, Electrical Engineering, Faculty of Engineering and Built Environment, Tshwane University of Technology, P.M.B. X680, Pretoria, South Africa
[3]Photonic Center, Council for Scientific and Industrial Research, Pretoria, South Africa

Abstract. A preliminary investigation was conducted to choose process parameters for laser surface alloying of a novel high-entropy alloy-based composite coating on a steel substrate. The chosen ranges for laser power, scanning speed and powder feed rate are 1500 to 2500 W, 0.4 to 0.8 m/min ute and 0.14 to 0.24 g/minute, respectively. The study examined the effect of powder feed rate and scanning speed on the properties of single beads. B eads' geometrical properties were measured, from which dilution percentage and aspect ratio were calculated. The correlation between microstructure and hardness value was also investigated. The highest combination of desired properties was achieved at 1500 W, 0.4 m/minute and 0.14 g/minute parameter settings. The bead deposited at the optimal condition resulted in dilution percentage, aspect ratio, and hardness value of 80.16%, 14.47, and 447.47 ± 6.60 $HV_{0.3}$, respectively. It hardness profile across deposited layer interface revealed that hardness values decreased across bead-heat affected zone-substrate interface in the order: 447.47 ± 6.60 $HV_{0.3}$ > 339 ± 36.93 $HV_{0.3}$ >155.3 ± 1.01 $HV_{0.3}$. Scanning electron microscopy revealed excellent bead-substrate melt pool mixing, resulting in good interfacial bonding, cracking, and pore-free microstructure.

1 Introduction

Heavy-duty machine parts engaged in mechanized earth-cutting or moving operations in mining, agriculture, and construction industries are made of steel. Unfortunately, steel corrodes and wears out after long and harsh service life conditions [1]. Repairing worn-out parts has become a hot topic in the operational and repair industries and is achieved by various surface engineering modification methods such as induction melting, plasma coating, and laser material processing. Depending on the layer thickness of a deposited coating, it is

* Correspoding author: ayo.alabi@ymail.com

classified as a clad or surface alloyed layer. Laser surface alloying is specifically useful in refurbishing worn steel parts, saving tons of useful steel, reducing costs of production and transporting new spare parts. It is also used to deposit coatings with exceptional bonding strength and a low heat-affected zone due to localized heating and rapid cooling rates, despite their high energy density. Furthermore, the process addresses high chances of segregation in the melt pool and thermal distortion of coated parts associated with other surface engineering modification processes due to the high heat input [2, 3].

Much emphasis has been put on refurbishing worn machine parts made of steel by laser surface alloying because it offers cost effective repair of damaged surfaces by powder filler materials. Moreover, due to the high energy density and quenching effect associated with laser surface alloying process by directed energy deposition, multicomponent materials can be melted and refined microstructures are often achieved [1, 2]. It has been reported that the geometrical, morphological, microstructural and mechanical properties of laser surface alloyed layers are significantly influenced by process parameters [3, 4]. This has prompted research interest to improve forming quality and geometry of laser surface alloyed layers, which are needed for superior surface and mechanical properties in refurbished machine parts to be subjected to extreme environment.

Unlike the laser cladding process that has been extensively investigated, only a few correlations have been established for the properties of coatings deposited by laser surface alloying and process parameters. Many authors also focused on optimizing a single property at a time. Hence, much remains to be done in this area. Improved results can be achieved by optimizing process parameters such as powder composition, feed rate, scanning speed, and laser power, especially when laying multi-component powders [5]. Wu, et al. [6] studied the influence of titanium carbide on the wear resistance of laser surface alloyed FeCoCrAlTiNi on 304 stainless steel and achieved better wear resistance at a higher reinforcement content. Wear characteristics of laser surface alloyed FeCoCrAlCu high-entropy alloy (HEA) reinforced with titanium carbide and deposited on steel was also investigated by Jiang, et al. [7], and high reinforcement content up to 50 wt.% was added. Enhancements in hardness and wear resistance were observed as the reinforcement content increase, achieving optimal properties for the coating at 50 wt.% titanium carbide addition. Siddiqui and Dubey [8] developed models that optimized hardness and erosion resistance of laser surface alloyed $Al_xCu_{0.5}FeNiTi$ on a AA1050 aluminium substrate from experimental data. The models wer e used to achieveimproved hardness and erosion resistance of 11.56 and 22.44%, respective ly. The objective of this study is to explore the feasibility of laser surface alloying a new HEA-based composite coating on a steel baseplate. The composition of the coating is $Nb_{11.2}Cr_{22.2}Co_{22.2}Ni_{22.2}Cu_{22.2}$/12.5% titanium nitride/12.5% vanadium carbide. The study will examine the effect of processing parameter settings on the geometrical properties and quality of beads. These will be related to the formation of robust microstructures required for impro ved mechanical properties of the laser surface alloyed coating.

2 Methodology

2.1 Laser surface alloying process

Beads were deposited on a mild steel baseplate using an IGP fiber laser. The baseplate was sandblasted, washed with liquid soap, acetone, and air dried to remove contaminants and increase laser beam absorption prior to the surface alloying process. Niobium of particles size D50 less than 45 µm and chromium, cobalt, nickel, and copper powders of particle sizes – 45 + 90 µm were weighed to form an HEA composition and mixed in a tubular mixer at 74 rpm for 10 hours. Thereafter, 75 wt.% of the HEA composition, 12.5 wt.% of titanium nitride (D50 less than 45 µm), and 12.5 wt.% of vanadium carbide (D50 less than 45 µm) were weighed and mixed in a tubular mixer for 3 hours (Figure 1).

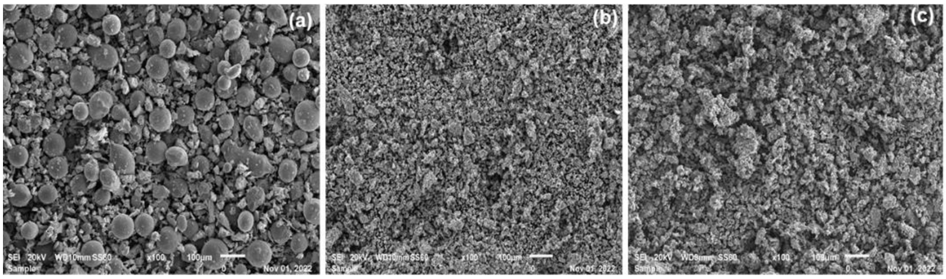

Fig. 1: Morphology of powders used (a) $Nb_{11.2}Cr_{22.2}Co_{22.2}Ni_{22.2}Cu_{22.2}$ HEA (b) Titanium nitride (TiN) (c) Vanadium carbide (VC).

2.2 Process parameter, bead geometrical studies and characterization

The beads were fabricated according to various processing parameter settings presented in Table 1. This was done at a constant carrier gas flow rate of 2 l/min, spot diameter of 3 mm and central purge gas flow rate of 20 l/min. The parameters were chosen from related literature [9-11]. The articles reported that powder feed rate (PFR), laser power (LP) and scanning speed (SS) are among the influential parameters in directed energy deposition. Therefore, those factors were considered in this preliminary study. PFR was varied at constant LP and SS of 1500 W and 0.4 m/min and SS was varied at constant LP and PFR of 2500 W and 0.24 g/min.

Table 1: Factors and levels for parametric study.

Process Parameters	Unit	Levels		
		1	**2**	**3**
Laser power	W	1500	-	2500
Scanning speed	m/minute	0.4	0.6	0.8
Powder feed rate	g/minute	0.14	0.19	0.24

The dilution percentage (DP) and aspect ratio (AR) of deposited beads were calculated from equations 1 and 2 using deposited bead geometrical variables shown in Figure 2. DP is a measure of degree of mixing between the substrate and deposited filler materials, while AR gives the extent of bead spread with respect to its height [3].

$$Dilution\ Percentage = \frac{d}{d+h} \times 100 \quad (1)$$

$$Aspect\ ratio = \frac{w}{h} \quad (2)$$

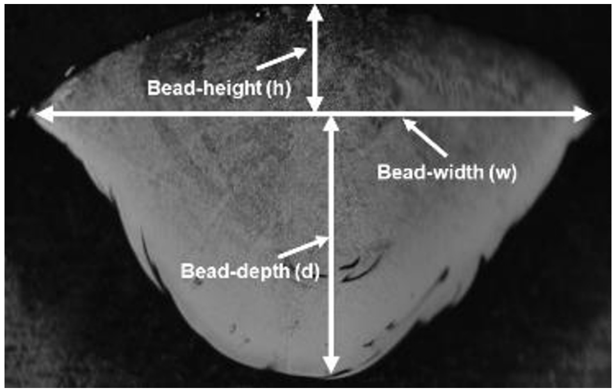

Fig. 2: Bead cross-section.

Samples were prepared according to ASTM E3-11 metallurgical standard procedures and etched using marble reagent [13]. Microstructural examinations were conducted using Olympus $BX_{51}M$ optical microscope and JEOL-JSM-6010 PLUS/LAM scanning electron microscope. The hardness of the samples was determined using a Zwick/Roell Indentec Vickers microhardness machine, recording an average of 10 indentations per sample, while stiffness measurement under a maximum load of 400 mN was conducted using Aton-paar, NHT^3 nanoindenter with Berkovich pyramid indenter. PANalytical Empyrean x-ray diffraction equipment was used to obtain diffractograms of the samples.

3 Result and discussion

Laser surface alloying is beneficial for repair and refurbishing by matching the properties of deposited coatings with those of worn steel parts. This involves tuning the geometrical, morphological, microstructural, and mechanical properties of coatings with those of worn metals to achieve similar properties that include but are not limited to surface topology, roughness, grain size, phases formed and their distribution. It is also important to achieve similar mechanical properties such as hardness, strength, ductility and stiffness for deposited coating and worn parts in some cases. The target in certain situations may be achieving coatings with enhanced physical or chemical properties and all these can be achieved by varying process parameters, which can influence solidification dynamics, such that it modulate final bead properties depending on how the change affects the melt pool's cooling rate, solid-liquid interface temperature gradient, and solidification velocity [14, 15].

3.1 Effect of process parameters on bead geometrical properties and forming quality

The graphs in Figure 3 present the effect of process parameter settings on bead geometry, whereas Figure 4 depicts micrographs that showed the forming quality of bead sections deposited under various process parameter settings. At constant LP and SS of 1500 W and 0.4 m/min, reduced bead-high (h) and bead-width (w) of 107.66 and 1547.37 µm were recorded for the bead fabricated at 0.14 g/min PFR, these measurements are comparatively lower than h and w values of 345.55 and 1685.88 µm measured in the bead deposited at 0.24 g/min PFR. The penetration depth also dropped from 434.93 µm for bead deposited at 0.14 g/min to 376.08 µm when the PFR setting was 0.24 g/min. This demonstrated that varying the PFR can impact the geometrical parameters of deposited beads during surface laser alloying.

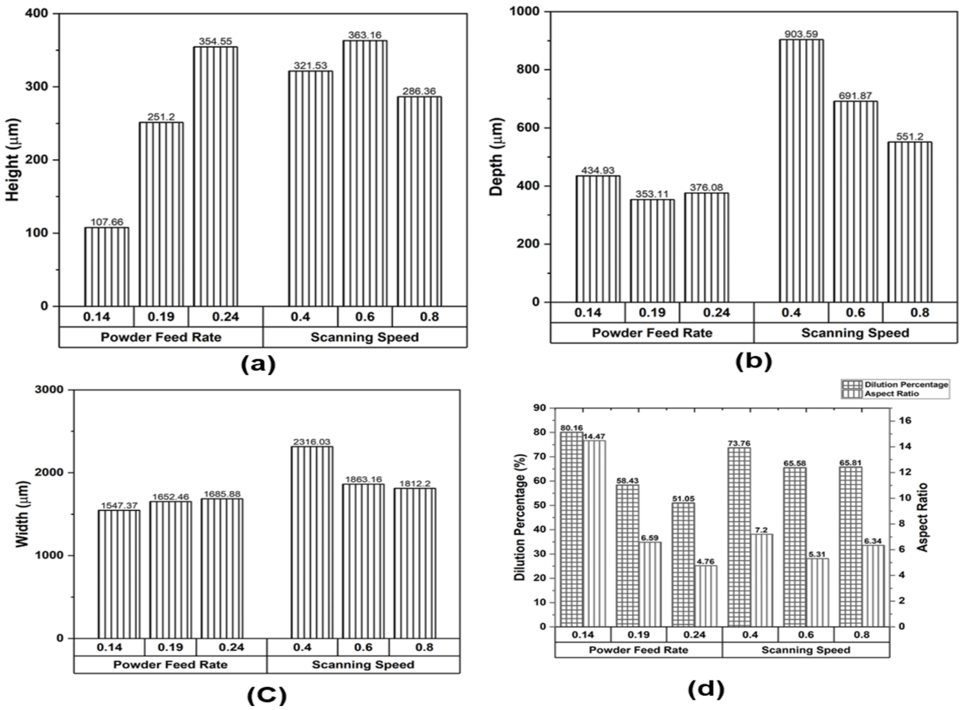

Fig. 3: Effect of process parameters variation on the bead geometry.

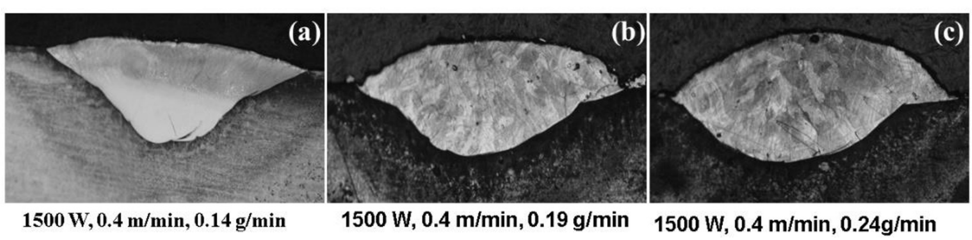

Fig. 4: Beads cross-sections at varied powder feed rate.

The bead deposited at 0.14 g/min was shorter and narrower due to less volume of deposited powder and high heat transfer at the melt-substrate interface that melted a larger volume fraction of the substrate. This led to a combination of high AR and DP needed for desired geometry and forming quality in laser surface alloying [3]. However, a higher and wider bead was observed at of 0.24 g/min PFR setting, but d reduced from 434.93 μm for beat built at 0.14 g/min to 376.08 μm for bead deposited at 0.24 g/min PFR. This could be due to the shadowing effect of more powder flow, which absorbs most of the heat input from the substrate's surface, decreasing the proportion of substrate melted [10]. The values of DP and AR were also reduced stepwise at different PFR values, as these parameters depend on d, h, and w. It was found that d greatly influences DP, and PFR affects DP by influencing d. Additionally, PFR had a greater impact on h than w, resulting in a reduced AR of 4.76 for beat deposited at 0.24 g/min compared to 14.37 computed for bead fabricated at 0.14 g/min due to increased h.

The study revealed that when SS was varied at a constant PFR and LP of 0.24 g/min and 2500 W, good forming quality was also achieved as shown in Figure 5, however, d, w, and h all decreased as presented in Figure 3. This is because of the inverse correlation between SS with heat input and interaction time that decreased the volume of melted deposited powder and substrate [16]. Additionally, DP and AR values decreased, from 72.26% and 7.2 at 0.4 m/min to 65.81% and 6.34 at 0.8 m/min, respectively. Suggesting that increasing SS at constant LP and PFR decreases bead geometrical parameters. Cui, et al. [17] observed similar trend when HEA powder was used for surface alloying on steel substrate.

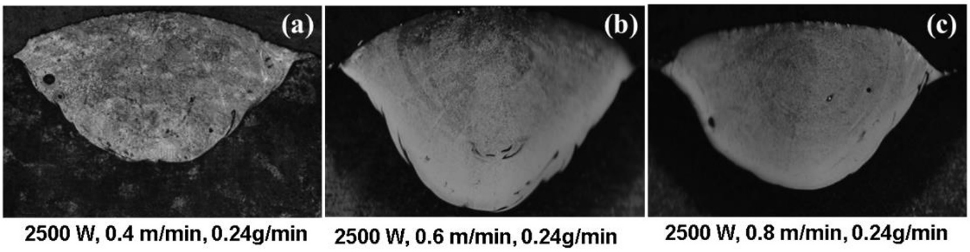

Fig. 5: Bead cross-sections at varied scanning speed.

3.2 Process parameters, microstructure and mechanical properties correlation

Bead micrographs revealed different zones dominated by columnar, equiaxed and cellular grains as process parameters were varied. The microstructural differences greatly influenced the mechanical properties of deposited beads.

3.2.1 The effect of PFR on beads' microstructural evolution

Jelvani, et al. [18] reported that the cooling rate and solidification velocity of the directed energy deposited melt pool are important in determining its solidification microstructure. However, there is no established relationship between the PFR and the two factors.
Moreover, these factors are functions of temperature gradient and rate of grain growth, which are greatly affected by the shadowing effect of powder flow into melt pool. Therefore, it could be argued that PFR can influence solidification parameters such as grain size, microstructural and phases distribution since they can significantly change the dynamics of melt-substrate interface heat transfer, melt heat input, temperature gradient and rate of grain growth due to the powder flow shadowing effect discussed earlier [18].

Figure 6a and c compared the microstructures formed at PFR of 0.14 g/min and 0.24 g/min. The beads were deposited at constant LP and SS of 1500W and 0.4 m/min. It was observed that at 0.14 g/min PFR, the grain size changed from columnar at the upper part (Fi gure 6a) to more refined grains with reinforcements pushed to the grain boundaries, moving from the center to the lower part of the bead (Figure 6b). At 0.24 g/min (Figure 6d), the dominant microstructure (zone B) revealed a comparatively inhomogeneous microstructure with smaller grain size but less defined grain boundaries. Zone A (Figure 6d) also showed partial precipitation of ceramic layers covering the intergranular and bulk of the grains. This can be attributed to the effect of PFR on the melt pool's temperature gradient and cooling rate [18, 19]. Lee, et al. [20] also observed a change in the microstructure of laser surface alloyed layer as PFR was varied.

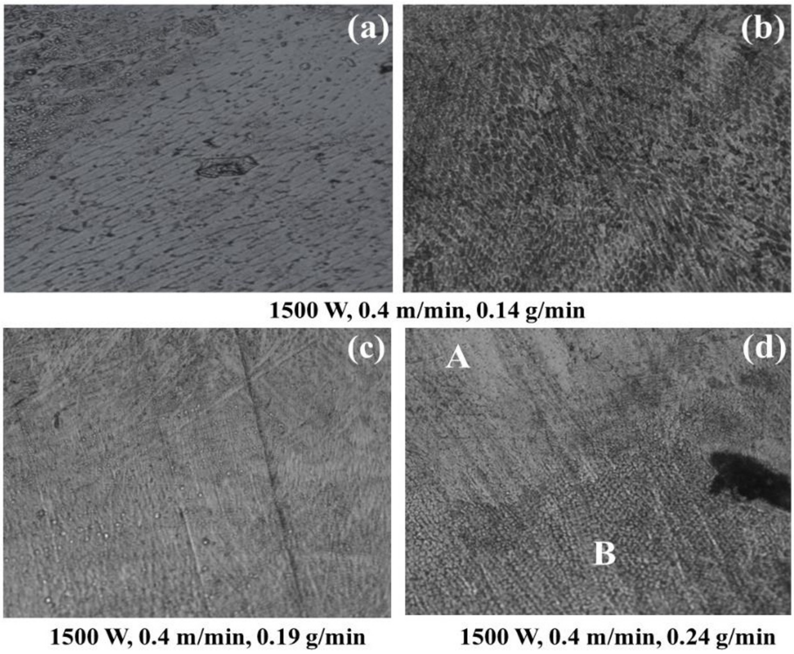

Fig. 6: Bead micrograph at varied powder feed rate.

3.2.2 The effect of SS on beads' microstructural evolution

The effect of varying SS at constant LP and PFR of 2500 W and 0.24 g/min on the bead's microstructural evolution was examined, and Figure 7 showed a major transformation between structures observed at 0.4 and 0.8 m/min. At 0.4 m/min Figure 7a, the bulk of the solidification structure was mainly covered by ceramic precipitates, while, at 0.8 m/min Figure 7c, a structure with comparably lesser ceramic precipitates, well defined grain boundaries, with distribution of equiaxed and columnar grains was shown.

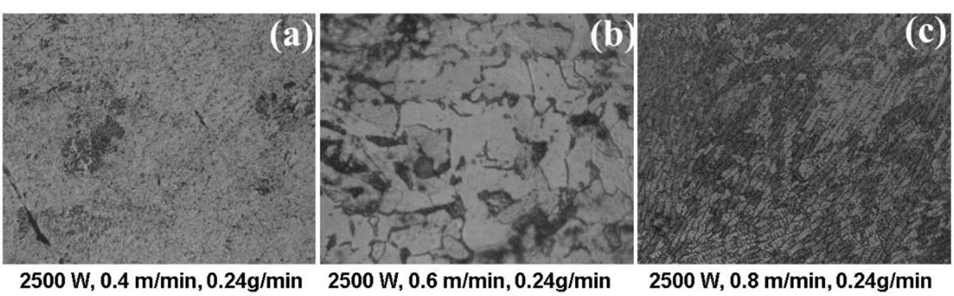

Fig. 7: Bead micrograph at varied scanning speed.

The finding is attributed to shorter laser-powder dwell time that promoted faster cooling rate at higher value of SS. This resulted in partial dissolution and precipitation of reinforcin g ceramics at 0.8 m/min. compared to an almost complete dissolution and precipitation obse rved at 0.4 m/min due to longer interaction time [15].

3.2.3 The effect of PFR and SS on beads' mechanical properties

Figure 8 presents the microhardness and stiffness of beads as functions of process parameters variation.

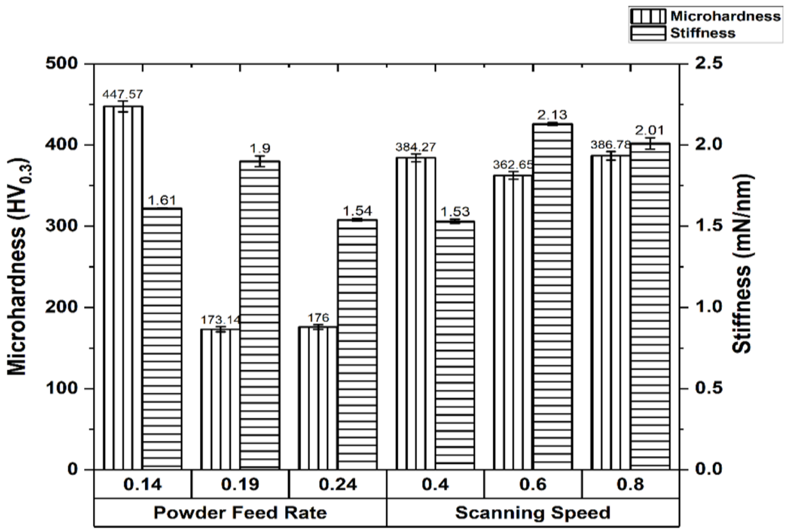

Fig. 8: Effect of process parameters on mechanical properties.

At constant LP and SS values of 1500 W and 0.4 m/min, the hardness values of beads deposited at PFR of 0.14 and 0.24 g/min were compared. The result showed a considerable decrease in microhardness value from 447.57 ± 6.60 $HV_{0.3}$ at 0.14 g/min to 176.00 ± 2.80 $HV_{0.3}$. at 0.24 g/min. The observation is contrary to the popular assertion in the literature that shows a correlation between grain refinement and an increase in the hardness value of metal/ceramic composites, which is usually backed by the Hall-Petch's relationship [21, 22]. The observation is due to the shadowing effect of injecting more powder into the melt pool at constant LP and SS, resulting in decreased temperature transfer at melt-substrate interface and melt's temperature gradient that led to a faster cooling rate. The rapid grain nucleation and solidification considerably affects the dissolution, precipitation, and dispersion time of reinforcing ceramics, and decreases the strengthening effect of well-dispersed hard phases. HEA-based composites beads' hardness values cannot be explained solely by grain refinement but also depend on the type and distribution of solidification structures formed. Therefore, since process parameters can greatly affect the heat input, cooling rate, and interaction time of the direct energy-deposited melt's pool, they can affect solidification structures [15, 18]. Conversely, the limited dissolution and precipitation time available, affected the dispersion density of hard ceramics in the bead and may possibly be the reason for lower hardness value observed at 0.24 g/min.

At constant LP and PFR of 2500 W and 0.24 g/min, a hardness value of 386.78 ± 5.26 $HV_{0.3}$ at 0.8 m/min was recorded, which is slightly higher than the 384.27 ± 4.91 $HV_{0.3}$ exhibited by the bead deposited at 0.4 m/min. The grain refinement observed at a SS of 0.8 m/min can also be attributed to the shorter available interaction and solidification time of the melt [23]. However, the grain refinement at a SS of 0.8 m/min improved the hardness value of bead, unlike the refining effect induced by PFR. This is in line with the Hall Petch's relationship mentioned previously.

Figure 8 also displays the plots for the stiffness of beads at different process parameter settings. A similar trend to that observed in beads' hardness was noted for stiffness readings for samples deposited under identical process parameter settings; thereby, verifying the accuracy of the recorded hardness data, as stiffness and hardness are both influenced by the same strengthening mechanisms in composite materials [24]. Although, hardness and stiffness measure materials' resistance to plastic and elastic deformation, respectively.

The results presented so far confirmed that bead geometry, morphology, microstructure and mechanical properties strongly depend on laser surface alloying process parameters and can be easily varied and optimized to modulate the properties of deposited layers to match those of worn metal parts to be refurbished. The findings affirmed the assertion of Siddiqui and Dubey [5] that claimed that process parameters optimization is often needed to achieve desirable properties of deposited layers in laser surface alloying.

In this preliminary study, the bead deposited at parameter settings of 1500 W, 0.4 m/min and 0.14 g/min showed comparatively better DP, AR, and microhardness value. Its hardness values across the bead's cross-section, heat affected zone (HAZ) and steel substrate were carefully reviewed and a hardness value profile plotted to understand how laser surface alloying process affects different zones of bead-substrate interface. Although hardness value increased when measured from upper to lower part of the bead, an average hardness value of 447.57 ± 6.60 $HV_{0.3}$ was recorded, with a standard mean error of 6.60 $HV_{0.3}$, revealing a slight variation in hardness values at different zones of the bead. This is attributable to microstructural distribution of columnar and equiaxed dendrites at upper and lower parts of the bead. Figure 9c and d show the SEM/EDS image of the bead with the highest hardness value. In addition, the bead also gave about 3 times better hardness value than that of the substrate (155.3 ± 1.01 $HV_{0.3}$). Differences in hardness values distribution across HAZ were also observed. An average of 339 ± 36.93 $HV_{0.3}$ revealed that hardness value distribution changed greatly across the HAZ. Higher hardness values are observed closer to the fusion line shown in Figure 9a and b and gradually decreased towards the substrate; indicating that elemental diffusion into the HAZ occurred during the dilution process. This could have led to the formation of solid-solution phases that resulted in relatively higher hardness values in the HAZ compared to the substrate [25].

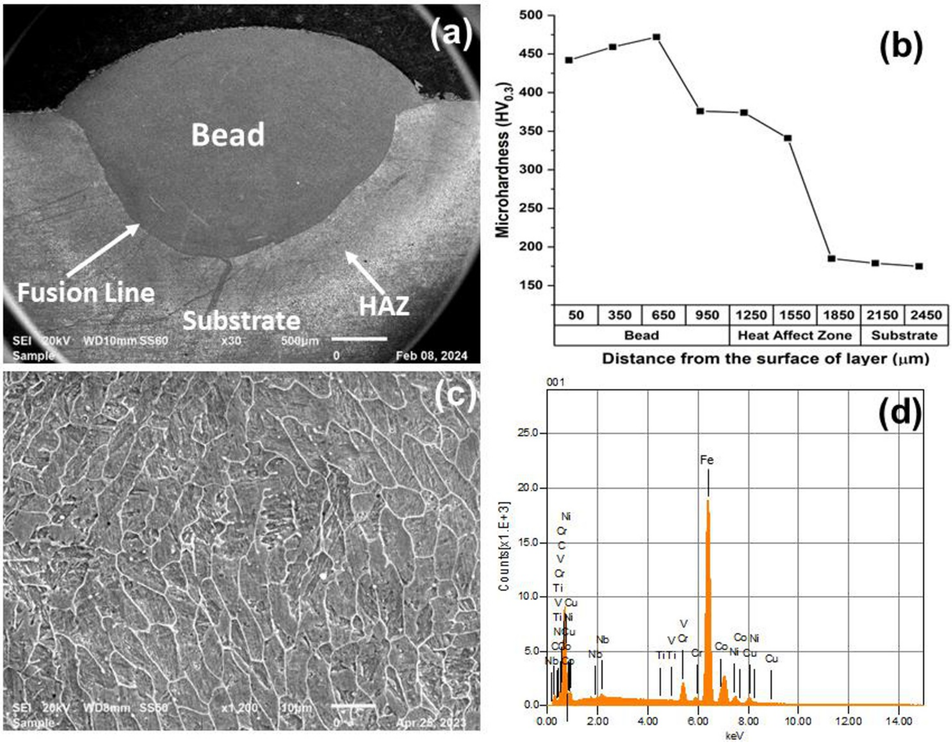

Fig. 9: SEM images of bead (a) cross section (c) microstructure (d) EDS and (b) hardness profile across bead, HAZ and substrate.

The ranges of process parameters chosen for this preliminary study revealed that reasonable DP and AR of the laser surface alloyed layer on a steel substrate is achievable and parameter settings can be varied or optimized to modulated geometrical, morphological and mechanical properties. Thus, making the newly developed HEA-based composite promising for repairs of worn steel part surfaces.

4 Conclusion

Herein, a novel HEA-based composite for surface engineering applications was reported. A preliminary study was conducted using certain ranges of direct energy deposition process parameters from related literature that gave robust, crack- and pore-free coatings on steel baseplate with desirable geometrical, morphological, microstructural, and mechanical properties that could be modulated by process parameter optimization to match those of worn steel parts to be repaired by laser surface alloying. The variation of PFR and SS at low and high process parameter settings resulted in the deposition of beads with combinations of good DPs, ARs, and hardness values of 80.16%, 14.47 and 447.47 ± 6.60 $HV_{0.3}$ at (1500 W, 0.4 m/min. and 0.14 g/min), and 73.76%, 7.2 and 384.27 ± 4.91 $HV_{0.3}$ at (2500 W, 0.4 m/min and 0.24 g/min), respectively. However, a slightly higher hardness value of 386.76 ± 5.26 $HV_{0.3}$ was exhibited by the bead deposited at 0.8 m/min, 2500 W and 0.4 g/min parameter settings, suggesting that the hardness value of coatings may depend on other factors than those discussed in this study. A hardness profile also revealed that hardness decreased in the order: bead > HAZ > substrate, and the coating exhibited about a three-times improvement in hardness value over that of the steel substrate. In conclusion, the preliminary study established that laser surface alloying of the novel HEA-based composite is achievable within the chosen ranges of process parameters. The investigation also demonstrated that beads' properties greatly depend on process parameter settings, which can be varied or optimized to modulate surface alloyed layer properties to match those of worn steel parts to be repaired.

References

1. B. Du, Z. Zhang, S. Suo, X. Li, and H. Deng, Surf. Rev. Lett. **28**, 2050033 (2021).
2. B. Manjunath, A. Vinod, K. Abhinav, S. Verma, and M. R. Sankar, Mater. Today Proc. **26**, 1108-1112 (2020).
3. A. A. Siddiqui and A. K. Dubey, Mater. Today Proc. **44**, 1108-1110 (2021).
4. Y. Huang, Y. Hu, M. Zhang, C. Mao, K. Wang, Y. Tong, J. Zhang, and K. Li, J. Therm. Spray Tech. **31**, 1985 - 2000 (2022).
5. A. A. Siddiqui and A. K. Dubey, Optics Laser Technol. **134**, 106619 (2021).
6. C. Wu, T. Xu, Z. Wang, C. Zhang, S. Zhang, C. Ni, and D. Zhang, Ceram. Int. **48**, 20690-20698 (2022).
7. P. Jiang, C. Zhang, S. Zhang, J. Zhang, J. Chen, and Y. Liu, Mater. Chem. Phys. **255**, 123571 (2020).
8. A. A. Siddiqui and A. K. Dubey, J. Mater. Eng. Perform. **29** (10), 6761- 6773 (2020).
9. R. N. Elshaer, A. M. Elshazli, A. H. A. Hussein, and S. R. Al-Sayed, Int. J. Adv. Manuf. Technol. **121**, 5139 - 5154 (2022).
10. E. Figueredo, L. Apolinario, M. Santos, A. Silva, J. Avila, M. Lima, and T. Santos, J. Mater. Eng. Perform. **30**, 3298- 3312 (2021).
11. H. Li, W. Fu, T. Chen, Y. Huang, Z. Ning, J. Sun, H. Bai, X. Dai, H. Fan, and A. H. Ngan, J. Alloys Compd. **924**, 166513 (2022).
12. R. Baboian, Corrosion tests and standards: application and interpretation. ASTM international, 2005.
13. ASTM E3-11, Standard guide for preparation of metallographic specimens, ASTM International: West Conshohocken, PA, USA, 2017.
14. S. Anandan, S. Pityana, and J. D. Majumdar, Mater. Sci. Eng. **536**, 159-169 (2012).
15. A. Alhuzaim, S. Imbrogno, and M. M. Attallah, J. Alloys Compd. **872**, 159588 (2021).
16. A. B. B. Henriques, P. L. de Aguiar, R. G. dos Santos, and J. Miagava, *Evaluation of process parameters modifications on directed energy deposition manufactured parts obtained in a hybrid additive manufacturing machine,* in Proceedings of the International Manufacturing Science and Engineering Conference, MSEC, V002T05A030 June 2022, Detroit, USA (2022).
17. W. Cui, H. Wang, D. Shao, B. Han, and J. Lin, *Analysis of influencing factors and experimental study on properties of laser cladding layer,* in the Proceedings of IOP Conference Series: Materials Science and Engineering, MSE, 032016 October 2019, Beijing, China (2019).
18. S. Jelvani, R. S. Razavi, M. Barekat, M. R. Dehnavi, and M. Erfanmanesh, Optics Laser Technol. **120**, 105761 (2019).
19. J. Shao, G. Yu, X. He, S. Li, R. Chen, and Y. Zhao, Optics & Laser Technology **119**, 105662 (2019).
20. K.-H. Lee, S.-W. Choi, J. Suh, and C.-Y. Kang, Mater. Des. **95**, 173-182 (2016).
21. C. Tan, J. Zou, D. Wang, W. Ma, and K. Zhou, Compos. Part B: Engin. **236**, 109820 (2022).
22. M. Ostolaza, J. I. Arrizubieta, A. Lamikiz, and E. Ukar, Surf. Coat. Technol. **463**, 129538 (2023).
23. D.R. Liu, S. Wang, and W. Yan, Mater. Des. **194**, 108919 (2020).
24. G. Ziegenhain and H. M. Urbassek, Philos. Mag. **89** , 2225-2238 (2009).

25. M. Feng, T. Lin, G. Lian, C. Chen, and X. Huang, J. Mater. Res. Technol. **28**, 3835-3848 (2024).